Performance Optimizing Gust Load Alleviation Control of Flexible Wing Aircraft

Kelley E. Hashemi*

Universities Space Research Association, Moffett Field, CA, 94035

Nhan T. Nguyen†

NASA Ames Research Center, Moffett Field, CA, 94035

Michael Drew‡

Stinger Ghaffarian Technologies, Inc., Moffett Field, CA, 94035

Daniel Chaparro§

MORI Associates, Moffett Field, CA, 94035

Eric Ting¶

NASA Ames Research Center, Moffett Field, CA, 94035

This paper details a control design for flexible wing aircraft that attempts to minimize the load induced by gust disturbance. Wing root bending moment is taken as an available measure of gust load and is used in a performance optimizing cost function to determine the load-alleviating control signal. However, both the disturbance signal and system matrices associated with wing root bending moment are unknown quantities. Estimates are instead generated online and used to complete the control formulation. Use of the time-varying matrix estimates in the performance index necessitates solving a Riccati equation at each time step and results in time-varying control gains. The control system is simulated on a reduced stiffness transport aircraft equipped with a wing shaping flap design and is seen to significantly reduce the load metric.

Nomenclature

M_y	Wing root bending moment, ft-lb
y	Accelerometer output, ft/s^2
w	Gust disturbance vector
ε_r	Rigid dynamics predictor model error
ε_M	Wing root bending moment estimation error

Subscript

r	Rigid dynamics quantity
e	Elastic dynamics quantity

*NASA Postdoctoal Fellow, Intelligent Systems Division, AIAA Member, kelley.e.hashemi@nasa.gov.

†Technical Group Lead and Research Scientist, Intelligent Systems Division, AIAA Associate Fellow, nhan.t.nguyen@nasa.gov.

‡Research Engineer, Stinger Ghaffarian Technologies, Inc., NASA Ames Research Center, michael.c.drew@nasa.gov.

§Research Engineer, MORI Associates, NASA Ames Research Center, AIAA Member, daniel.chaparroespinoza@nasa.gov.

¶Research Engineer, Intelligent Systems Division, eric.b.ting@nasa.gov.

I. Introduction

The development of increasingly flexible flight vehicles has opened the possibility of in-flight tailoring to improve aerodynamic performance. Benefits such as reduced drag and decreased fuel consumption could be achieved by reshaping the flexible structure throughout the flight envelope. However, the same structural flexibility that enables such benefits also makes the vehicle more susceptible aeroelastic disturbances and instability. One option for managing the aeroelastic behavior of the vehicle is through active control system design. Ideally, the control system could be made to both suppress undesirable motion and shape the flexible structure in pursuit of improved performance goals.

In this investigation the disturbance effect of wind gust on a flexible wing aircraft is considered. A gust load alleviation (GLA) controller is designed to reduce the loads induced by gust by making use of wing shaping control surfaces distributed along the trailing edge of the wing. Use of the GLA controller is then shown to significantly reduce the load imparted by the gust–assessed through measurement of the wing root bending moment. The GLA control design is obtained from optimization of a multi-objective cost function involving unknown quantities including the disturbance signal and wing root bending moment system matrices. Estimates of the unknown quantities must be generated online and used to complete the control formulation. The presence of the time-varying estimates in the optimal control solution requires that a Riccati equation be solved at each time step to form time-varying GLA control signal gains.

The multi-objective optimal control approach used here for the GLA controller has been previously used to facilitate other performance-enhancing aircraft control designs.[1–4] In particular the technique has been show to be effective for both drag minimization[1,2] and maneuver load alleviation.[3] However, these implementations relied on all quantities required for control formulation being known. The case of unknown quantities in the performance metric has also been considered in the context of an adaptive control system,[4] though without the effect of a disturbance.

The GLA control design is demonstrated in simulation of gust-disturbed level flight of a flexible wing Generic Transport Model (GTM). The GTM is augmented with a Variable Camber Continuous Trailing Edge Flap (VCCTEF) control surface design that is used here to facilitate wing shaping for load alleviation. The VCCTEF concept is a novel trailing edge design that is formed by multiple, individually articulated spanwise flap segments that are joined by elastomer transition sections to create a continuous surface. This control surface design was proposed as a way to improve aerodynamic performance and has since been investigated for use with a range of flight performance-improving control designs.[5–8]

The paper is organized as follows: A description of the problem statement, specific to aircraft gust disturbance, is given in Section II. Section III then presents the multi-objective optimal control formulation for GLA and describes how unknown quantities are to be estimated. Details of the GTM implementation are provided in Section IV along with simulation results of the GLA controller, and some concluding remarks are provided in Section V.

II. Problem Formulation

Here, consider the problem of controlling a linear, aeroservoelastic model of an aircraft subject to an exogenous disturbance representing gust. The aircraft model is partitioned based on states corresponding to the aircraft's rigid dynamics and the aircraft's elastic dynamics. Two separate control terms are used: $u_r \in \mathbb{R}$ for the elevator and $u_e \in \mathbb{R}^{n_v}$ for the VCCTEF control surface. The elevator is used to provided nominal flight trajectory tracking and the VCCTEF for GLA wing shaping. Measurements from vertical axis accelerometers and strain gauges measuring wing root bending moment are available as outputs.

A. Plant description

The partitioned dynamics of the plant are taken to be

$$\begin{bmatrix} \dot{x}_r \\ \dot{x}_e \end{bmatrix} = \begin{bmatrix} A_{rr} & A_{re} \\ A_{er} & A_{ee} \end{bmatrix} \begin{bmatrix} x_r \\ x_e \end{bmatrix} + \begin{bmatrix} B_{rr} & B_{re} \\ B_{er} & B_{ee} \end{bmatrix} \begin{bmatrix} u_r \\ u_e \end{bmatrix} + \begin{bmatrix} w_r \\ w_e \end{bmatrix} \tag{1}$$

where $w_r \in \mathbb{R}^{n_r}$ and $w_e \in \mathbb{R}^{n_e}$ represents disturbance vectors to the rigid and elastic subsystems, respectively. All matrices are fully known. The rigid body states $x_r \in \mathbb{R}^{n_r}$ are available directly, but the elastic states $x_e \in$

$\mathbb{R}^{n_e}$ must be estimated if they are to be used in the control implementation. Accelerometer measurements $y \in \mathbb{R}^{n_o}$ of the form

$$y = \begin{bmatrix} C_r & C_e \end{bmatrix} \begin{bmatrix} x_r \\ x_e \end{bmatrix} + \begin{bmatrix} D_r & D_e \end{bmatrix} \begin{bmatrix} u_r \\ u_e \end{bmatrix} + \begin{bmatrix} E_r & E_e \end{bmatrix} \begin{bmatrix} w_r \\ w_e \end{bmatrix} \tag{2}$$

are available for this purpose. The observed dynamics, which must utilize estimates of the unknown disturbances, are then expressed as

$$\begin{bmatrix} \dot{x}_r \\ \dot{\hat{x}}_e \end{bmatrix} = \begin{bmatrix} A_{rr} & A_{re} \\ A_{er} & A_{ee} \end{bmatrix} \begin{bmatrix} x_r \\ \hat{x}_e \end{bmatrix} + \begin{bmatrix} 0 \\ L_e \end{bmatrix} (y - \hat{y}) + \begin{bmatrix} B_{rr} & B_{re} \\ B_{er} & B_{ee} \end{bmatrix} \begin{bmatrix} u_r \\ u_e \end{bmatrix} + \begin{bmatrix} \hat{w}_r \\ \hat{w}_e \end{bmatrix} \tag{3}$$

where the estimated measurements are

$$\hat{y} = \begin{bmatrix} C_r & C_e \end{bmatrix} \begin{bmatrix} x_r \\ \hat{x}_e \end{bmatrix} + \begin{bmatrix} D_r & D_e \end{bmatrix} \begin{bmatrix} u_r \\ u_e \end{bmatrix} + \begin{bmatrix} E_r & E_e \end{bmatrix} \begin{bmatrix} \hat{w}_r \\ \hat{w}_e \end{bmatrix}. \tag{4}$$

The elastic observer gain L_e is the appropriately-sized portion of the observer gain computed using the entire A matrix in Eq. (1) and entire C matrix in Eq. (2).

Additionally, wing root bending moment $M_y \in \mathbb{R}$ is an available performance metric of the form

$$M_y = \begin{bmatrix} M_{x_r} & M_{x_e} \end{bmatrix} \begin{bmatrix} x_r \\ x_e \end{bmatrix} + \begin{bmatrix} M_{u_r} & M_{u_e} \end{bmatrix} \begin{bmatrix} u_r \\ u_e \end{bmatrix} + \begin{bmatrix} M_{w_r} & M_{w_e} \end{bmatrix} \begin{bmatrix} w_r \\ w_e \end{bmatrix}. \tag{5}$$

The M_x, M_u, and M_w matrices are unknown. An estimate of the performance metric is thus obtained from

$$\hat{M}_y = \begin{bmatrix} \hat{M}_{x_r} & \hat{M}_{x_e} \end{bmatrix} \begin{bmatrix} x_r \\ \hat{x}_e \end{bmatrix} + \begin{bmatrix} \hat{M}_{u_r} & \hat{M}_{u_e} \end{bmatrix} \begin{bmatrix} u_r \\ u_e \end{bmatrix} + \begin{bmatrix} \hat{M}_{w_r} & \hat{M}_{w_e} \end{bmatrix} \begin{bmatrix} \hat{w}_r \\ \hat{w}_e \end{bmatrix}. \tag{6}$$

Note that a more compact version of the state space system in Eqs. (3), (4), and (6) is given by

$$\begin{aligned} \dot{\hat{x}} &= A\hat{x} + L(y - \hat{y}) + B_r u_r + B_e u_e + \hat{w} \\ \hat{y} &= C\hat{x} + D_r u_r + D_e u_e + E\hat{w} \\ \hat{M}_y &= \hat{M}_x \hat{x} + \hat{M}_{u_r} u_r + \hat{M}_{u_e} u_e + \hat{M}_w \hat{w}. \end{aligned} \tag{7}$$

The implied matrix and vector definitions will be used moving forward.

B. Nominal controller

The rigid controller u_r is designed to provide nominal flight trajectory tracking. Here a standard LQR design, with servomechanism when necessary for tracking, is employed and used to track a desired flight path angle. It is designed based on rigid dynamics of the plant only which have full state availability. Specified in a form relevant to the complete control design, u_r is given by

$$u_r = \begin{bmatrix} K_x & 0 \end{bmatrix} \begin{bmatrix} x_r \\ \hat{x}_e \end{bmatrix} \triangleq K_{nom} \hat{x}, \tag{8}$$

as stabilization is the tracking goal considered.

III. Gust Load Alleviating Controller

The GLA control term u_e is determined from the optimal control solution of a multi-objective cost function that seeks to provide both aeroelastic stabilization and minimize wing root bending moment. The cost function uses separately-determined and time-varying estimates of the wing root bending moment system matrices. The control formulation as well as an estimation procedure for the system matrices is presented in the following section. Additionally, an estimate of the disturbance vector must be generated to complete the implementation. Two disturbance estimation procedures are presented here as well, one based on an adaptive formulation and one using an extended state observer.

A. Multi-objective formulation

The infinite time horizon cost function for the GLA controller is given by

$$\begin{aligned} J &= \lim_{t_f\to\infty} \frac{1}{2}\int_0^{t_f} \left[\hat{x}^T G_x^T Q G_x \hat{x} + u_e^T R_e u_e + q\hat{M}_y^2\right] dt \\ &= \lim_{t_f\to\infty} \frac{1}{2}\int_0^{t_f} \left[\hat{x}^T G_x^T Q G_x \hat{x} + u_e^T R_e u_e + q\left(\hat{M}_x\hat{x} + \hat{M}_{u_r}u_r + \hat{M}_{u_e}u_e + \hat{M}_w\hat{w}\right)^2\right] dt. \end{aligned} \tag{9}$$

where matrices $Q > 0$ and $R_e > 0$ as well as scalar $q > 0$ are weights available for the user to assign. Here $G_x = \text{blkdiag}(0, I)$ is a block diagonal matrix that picks out the elastic states only. Note that the estimates of the system matrices are used so that the final u_e expression does not contain unknown quantities and is implementable. The estimates will be generated separately and are temporarily treated as known but time-varying quantities in this formulation. Also note that the partially observed state vector $\hat{x}$ is used everywhere instead of the true state vector x as this is the quantity present in $\hat{M}_y$. The first term of the cost function is used to stabilize the elastic modes while the last term serves to minimize the estimate of wing root bending moment–the performance metric used to represent gust load.

Proceeding to solve the optimal control problem for u_e, the Hamiltonian is given by

$$\begin{aligned} H = \frac{1}{2}\hat{x}^T G_x^T Q G_x \hat{x} + \frac{1}{2}u_e^T R_e u_e + \frac{1}{2}q\left(\hat{M}_x\hat{x} + \hat{M}_{u_r}u_r + \hat{M}_{u_e}u_e + \hat{M}_w\hat{w}\right)^2 \\ + \lambda^T\left[A\hat{x} + B_r u_r + B_e u_e + \hat{w} + L(y - \hat{y})\right]. \end{aligned} \tag{10}$$

Closing the u_r loop and using the definition for $\hat{y}$ leaves

$$\begin{aligned} H = \frac{1}{2}\hat{x}^T G_x^T Q G_x \hat{x} + \frac{1}{2}u_e^T R_e u_e + \frac{1}{2}q\left(\hat{\tilde{M}}_x\hat{x} + \hat{M}_{u_e}u_e + \hat{M}_w\hat{w}\right)^2 \\ + \lambda^T\left[\tilde{A}\hat{x} + B_e u_e + \hat{w} + L(y - \tilde{C}\hat{x} - D_e u_e - E\hat{w})\right] \end{aligned} \tag{11}$$

where $\hat{\tilde{M}} = \hat{M}_x + \hat{M}_{u_r}K_{nom}$, $\tilde{A} = A + B_r K_{nom}$, and $\tilde{C} = C + D_r K_{nom}$. The necessary conditions of optimality are

$$\dot{\lambda} = \frac{-\partial H^T}{\partial \hat{x}} = -G_x^T Q G_x \hat{x} - q\hat{\tilde{M}}_x^T\left(\hat{\tilde{M}}_x\hat{x} + \hat{M}_{u_e}u_e + \hat{M}_w\hat{w}\right) - \bar{A}^T\lambda \tag{12}$$

and

$$\frac{\partial H^T}{\partial u_e} = R_e u_e + q\hat{M}_{u_e}^T\left(\hat{\tilde{M}}_x\hat{x} + \hat{M}_{u_e}u_e + \hat{M}_w\hat{w}\right) + \bar{B}^T\lambda = 0 \tag{13}$$

where $\bar{A} = \tilde{A} - L\tilde{C}$ and $\bar{B} = B_e - LD_e$. The resulting optimal control is thus

$$u_e = K_x\hat{x} + K_w\hat{w} + K_y y \tag{14}$$

where

$$K_x = -\bar{R}_e^{-1}\left(q\hat{M}_{u_e}^T\hat{\tilde{M}}_x + \bar{B}^T W\right) \tag{15}$$

$$K_w = -\bar{R}_e^{-1}\left(q\hat{M}_{u_e}^T\hat{M}_w + \bar{B}^T V_w\right) \tag{16}$$

$$K_y = -\bar{R}_e^{-1}\bar{B}^T V_y. \tag{17}$$

Additional definitions are given by

$$\bar{R}_e = q\hat{M}_{u_e}^T\hat{M}_{u_e} + R_e \tag{18}$$

$$V_w = \bar{V}^{-1}\left[-W - q\hat{\tilde{M}}_x^T\hat{M}_w + q\left(W\bar{B} + q\hat{\tilde{M}}_x^T\hat{M}_{u_e}\right)\bar{R}_e^{-1}\hat{M}_{u_e}^T\hat{M}_w\right] \tag{19}$$

$$V_y = -\bar{V}^{-1}WL \tag{20}$$

where $\bar{V} = (\bar{\bar{A}}^T - W\bar{B}\bar{R}_e^{-1}\bar{B}^T)$ and W is the solution to the Riccati equation

$$\bar{\bar{A}}^T W + W\bar{\bar{A}} + \dot{W} - W\bar{B}\bar{R}_e^{-1}\bar{B}^T W + \bar{Q} = 0 \tag{21}$$

with

$$\bar{\bar{A}} = \bar{A} - q\bar{B}\bar{R}_e^{-1}\hat{M}_{u_e}^T\hat{\tilde{M}}_x \tag{22}$$

$$\bar{Q} = G_x^T Q G_x + q\hat{\tilde{M}}_x^T\hat{\tilde{M}}_x - q^2\hat{\tilde{M}}_x^T\hat{M}_{u_e}\bar{R}_e^{-1}\hat{M}_{u_e}^T\hat{\tilde{M}}_x. \tag{23}$$

The differential Riccati equation shown in Eq. (21) would typically be solved backwards in time to obtain the solution $W(t)$. For implementation, a simplifying approximation will be made where the algebraic version of the equation with $\dot{W} = 0$ is solved instead for the constant solution W. This choice is justified by the reasonable assumption that the time-varying estimates involved in the Riccati equation converge to a constant value after a brief transient.

B. Estimation of performance metric system matrices

To separately estimate the wing root bending moment system matrices, consider the performance metric estimation error given by

$$\begin{aligned}\varepsilon_M &= \hat{M}_y - M_y \\ &= (\hat{M}_x\hat{x} + \hat{M}_u u + \hat{M}_w\hat{w}) - (M_x x + M_u u + M_w w).\end{aligned} \tag{24}$$

Add and subtract the quantities $M_x\hat{x}$ and $M_w\hat{w}$ to obtain

$$\varepsilon_M = \tilde{M}_x\hat{x} + M_x\tilde{x} + \tilde{M}_u u + \tilde{M}_w\hat{w} + M_w\tilde{w} \tag{25}$$

For a cost function of the form

$$J = \frac{1}{2}\varepsilon_M^T\varepsilon_M \tag{26}$$

calculate the partials

$$\frac{\partial J}{\partial\tilde{M}_x} = \hat{x}\varepsilon_M^T \qquad \frac{\partial J}{\partial\tilde{M}_{u_r}} = u_r\varepsilon_M^T \qquad \frac{\partial J}{\partial\tilde{M}_{u_e}} = u_e\varepsilon_M^T \qquad \frac{\partial J}{\partial\tilde{M}_w} = \hat{w}\varepsilon_M^T. \tag{27}$$

The gradient update laws become

$$\dot{\hat{M}}_x^T = -\Gamma_{M_x}\frac{\partial J}{\partial\tilde{M}_x} = -\Gamma_{M_x}\hat{x}\varepsilon_M^T \tag{28}$$

and similarly

$$\dot{\hat{M}}_{u_r}^T = -\Gamma_{M_{u_r}}u_r\varepsilon_M^T \qquad \dot{\hat{M}}_{u_e}^T = -\Gamma_{M_{u_e}}u_e\varepsilon_M^T \qquad \dot{\hat{M}}_w^T = -\Gamma_{M_w}\hat{w}\varepsilon_M^T \tag{29}$$

with $\Gamma_{M_x}, \Gamma_{M_{u_r}}, \Gamma_{M_{u_e}}, \Gamma_{M_w} > 0$. When implementing ε_M, however, recall that M_y is an available measurement.

C. Adaptive estimation of disturbance signal

To separately estimate the disturbance, construct a dynamics error term

$$\varepsilon_r = \dot{\hat{x}}_r - \dot{x}_r \tag{30}$$

where the actual closed loop dynamics are given by

$$\dot{x}_r = (A_{rr} + B_{rr}K_{nom})x_r + A_{re}x_e + B_e u_e + w_r. \tag{31}$$

and an estimated version, called the predictor model,[3] is given by

$$\dot{\hat{x}}_r = (A_{rr} + B_{rr}K_{nom})\hat{x}_r + A_{re}\hat{x}_e + B_e u_e + \hat{w}_r. \tag{32}$$

The dynamics error becomes

$$\varepsilon_r = (A_{rr} + B_{rr}K_{nom})(\hat{x}_r - x_r) + A_{re}(\hat{x}_e - x_e) + (\hat{w}_r - w_r). \tag{33}$$

Then construct the cost function

$$J = \frac{1}{2}\varepsilon_r^T \varepsilon_r + \frac{1}{2}\varepsilon_M^T \varepsilon_M \tag{34}$$

which can be minimized by selecting the gradient update laws

$$\begin{aligned} \dot{\hat{w}}_r^T &= -\Gamma_{w_r} \frac{\partial J}{\partial \hat{w}_r} = -\Gamma_{w_r}(\varepsilon_r^T + \hat{M}_{w_r}\epsilon_M^T) \\ \dot{\hat{w}}_e^T &= -\Gamma_{w_e} \frac{\partial J}{\partial \hat{w}_e} = -\Gamma_{w_e}(\hat{M}_{w_e}\epsilon_M^T) \end{aligned} \tag{35}$$

with $\Gamma_{w_r}, \Gamma_{w_e} > 0$. Note that when ε_r is needed for implementation, $\dot{\hat{x}}_r$ is assembled using Eq. (32) and $\dot{x}_r$ is a taken as a known quantity.

D. Disturbance estimation using extended state observer

Use of an extended state observer is another method of obtaining disturbance estimates from the available measurements. Here $\hat{w}$ is determined by appending the disturbance vector to the state and constructing an observer for the extended system. The structure of the extended system is given by

$$\begin{bmatrix} \dot{x} \\ \dot{w} \end{bmatrix} = \begin{bmatrix} A & I \\ 0 & 0 \end{bmatrix} \begin{bmatrix} x \\ w \end{bmatrix} + \begin{bmatrix} B \\ 0 \end{bmatrix} u + \begin{bmatrix} 0 \\ I \end{bmatrix} \dot{w} \tag{36}$$

$$y = \begin{bmatrix} C & E \end{bmatrix} \begin{bmatrix} x \\ w \end{bmatrix} + Du \tag{37}$$

while the extended observed dynamics are given by

$$\begin{bmatrix} \dot{\hat{x}} \\ \dot{\hat{w}} \end{bmatrix} = \begin{bmatrix} A & I \\ 0 & 0 \end{bmatrix} \begin{bmatrix} \hat{x} \\ \hat{w} \end{bmatrix} + \begin{bmatrix} B \\ 0 \end{bmatrix} u + \begin{bmatrix} L_x \\ L_w \end{bmatrix} (y - \hat{y}) \tag{38}$$

$$\hat{y} = \begin{bmatrix} C & E \end{bmatrix} \begin{bmatrix} \hat{x} \\ \hat{w} \end{bmatrix} + Du. \tag{39}$$

The observer gain matrix is computed using the extended A and C matrices in Eqs. (38) and (39). The estimate $\hat{w}$ is simply extracted from the estimated state vector.

Note that if some entries of the disturbance vector are known to remain zero then they can be removed from the extended state through the mapping

$$w_{nz} = W_{\text{map}} w \tag{40}$$

where w_{nz} contains only the nonzero portion of w. In this case the observed dynamics are given by

$$\begin{bmatrix} \dot{\hat{x}} \\ \dot{\hat{w}}_{nz} \end{bmatrix} = \begin{bmatrix} A & W_{\text{map}}^T \\ 0 & 0 \end{bmatrix} \begin{bmatrix} \hat{x} \\ \hat{w}_{nz} \end{bmatrix} + \begin{bmatrix} B \\ 0 \end{bmatrix} u + \begin{bmatrix} L_x \\ L_{w_{nz}} \end{bmatrix} (y - \hat{y}) \tag{41}$$

$$\hat{y} = \begin{bmatrix} C & EW_{\text{map}}^T \end{bmatrix} \begin{bmatrix} \hat{x} \\ \hat{w}_{nz} \end{bmatrix} + Du \tag{42}$$

and the disturbance estimate can be recovered from the estimated state vector according to $\hat{w} = W_{\text{map}}^T \hat{w}_{nz}$.

IV. Application to GTM

A. Aircraft model description

For this study a flexible wing version of the GTM is used to simulated the proposed gust load alleviation controller. Specifically, the longitudinal aircraft model associated with mid-cruise flight conditions and a 50% reduction in traditional stiffness properties is considered. The aircraft is equipped with the novel VCCTEF

actuation device which can be used to exploit the increased flexibility for performance gain through wing shaping. The VCCTEF is shown in Fig. 1 and consists of 16 flap segments distributed along the trailing edge of the wing. Each segment can be individually actuated. Further, each segment consists of three chordwise elements which can also be individually articulated. This feature, however, is not utilized in the present study and a given flap segment is deflected as a single unit. A flexible elastomer joint is placed in the gap between two adjacent flap segments to create a smooth trailing edge. Additional details of the VCCTEF can be found in Refs. 5–8. The aircraft is also equipped with two accelerometers per wing and a strain gauge near the wing root as shown in the same figure.

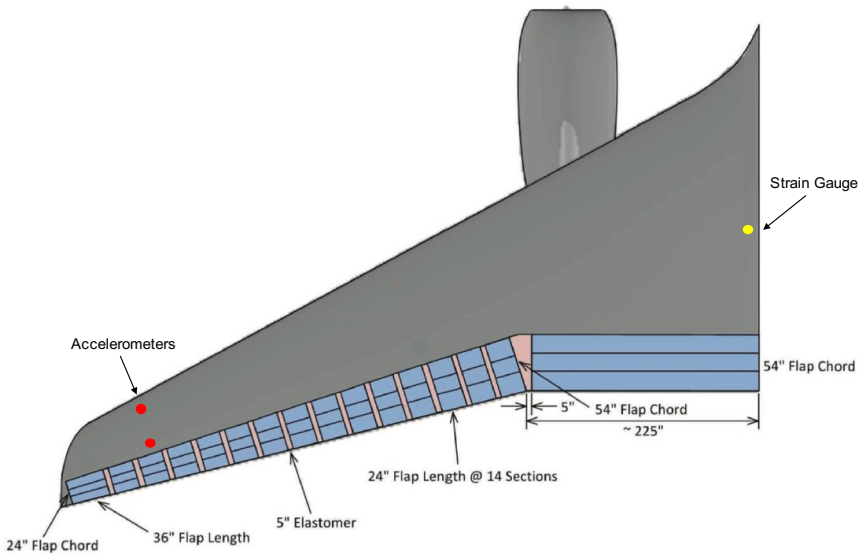

Figure 1. Illustration of 16 segment GTM VCCTEF design

The aircraft model consists of both rigid and aeroelastic dynamics coupled with the control input from the elevator and VCCTEF as well as the gust disturbance. The model can be partitioned into coupled rigid and elastic subsystems, as shown in Eq. (1), where the elastic states include modal position, modal velocity, and aerodynamic lag states arising from the R.T. Jones method of unsteady aerodynamic approximation. Dynamics of the actuators are neglected here. The number of modes included in the model can be changed such that if n_{mode} modes are retained, then $n_e = 6n_{\text{mode}}$.

While the VCCTEF segments can be commanded individually, constraints imposed by the actuator's design must be considered. Each segment must satisfy reasonable minimum and maximum deflection limits, but the primary limitation is imposed by the elastomer insert requiring that adjacent segments remain within roughly $\pm 2°$ of each other. This design constraint is addressed by reducing the number of control channels through the use of a shape function. Here a fourth-order Chebyshev polynomial is used to describe the total deflection profile of the VCCTEF and each time step. The shape implied by this function is then discretized to recover the 16 flap segment commands. Thus, the original 16-input system is reduced to a 4-virtual input system for control calculation and $u_e \in \mathbb{R}^{n_v}$ where $n_v = 4$. The Chebyshev polynomial shape function is given by

$$\delta_i = c_0 + c_1 k + c_2(2k^2 - 1) + c_3(4k^3 - 3k) \tag{43}$$

where $k = \frac{i-1}{n-1}$ for $i = 1...16$. Here δ_i is the deflection of the ith segment and c_j for $j = 0...(n_v - 1)$ are the virtual control variables. Use of the shape function helps create a smooth surface of deflections that is more likely to satisfy relative deflection limits than individual actuation.

B. Gust model

The Von Kármán turbulence model is used to continuously generate a vertical gust velocity from a random signal.[9] The instantaneous angle of attack for a wing section due to this velocity is approximated using

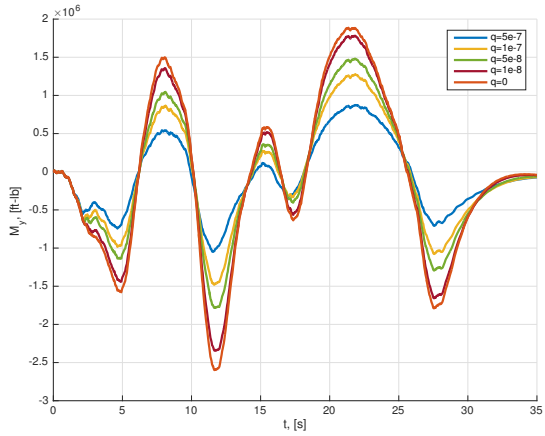

Figure 2. Wing root bending moment comparison with various q values

linear potential flow theory and an appropriate delay to account for the gust's travel time to the leading edge. Next the R.T. Jones approximation of the Küssner function is applied to the instantaneous angle of attack to obtain the section's unsteady lift, drag, and pitching moment coefficients due to the gust. Finally, the section loads of the wing are integrated to compute the aircraft loads due to gust. The resulting forces are coupled to both the aircraft flight dynamics and aeroelasticity leading to the gust-disturbed equations of motion given in Eqs. (1) and (2). A more detailed description of this process is provided in Ref. 10. Note that only a subset of the rigid body states and the elastic position states have gust disturbance contributions. All other entries of w are zeros. A mapping to extract only the nonzero entries as described in Eq. (40) can be used to reduce the size of the extended state observer if desired.

C. Simulation results

The following simulation results demonstrate the load alleviation capability of the GLA controller in response to a gust-like disturbance while the nominal controller attempts to maintain level flight at cruise conditions. The control input is calculated on a longitudinal model of the GTM with 5 elastic modes retained and simulated on a model with 10 modes retained. Elastic position, elastic velocity, and aerodynamic lag terms constitute the elastic portion of the system totaling $n_e = 30$ states for the control calculation model. The shape function utilizes $n_v = 4$ virtual control variables to prescribe commands to all VCCTEF segments. Two accelerometer measurements are used as output for the observer design and a single strain gauge provides the wing root bending moment. Settings for the GLA controller include $Q = 10I_{n_e}$ and $R_e = 5e6I_{n_v}$ while the choice of q will be analyzed subsequently. The gust disturbance is active for 30 seconds before decaying to zero. Use of the adaptive disturbance estimation scheme is considered first with learning rates for the estimated quantities selected as $\Gamma_{w_r} = 1e-11$ and $\Gamma_{w_r} = 1e-8$ as well as $\Gamma_{M_x} = 10$, $\Gamma_{M_{u_r}} = 10$, $\Gamma_{M_{u_e}} = 10$, and $\Gamma_{M_w} = 0.1$. The use of the disturbance estimate from the extended state observer is briefly considered subsequently.

Figure 2 shows the impact of changing the scalar weighting parameter q that precedes the wing root bending moment term in the cost function. As expected, the reduction in M_y from the case of $q = 0$ (i.e. GLA controller off) increases as the value is increased. However, the commanded VCCTEF deflections also increase and are unreasonably large for the $q = 5e-7$ case. The value $q = 1e-7$ is selected for demonstration purposes for the remainder of the paper. Note that for this value of q, M_y is reduced from an extremum of $-2.6e6$ ft-lb to one of $-1.481e6$ ft-lb which corresponds to a sizable 43% decrease.

The next set of figures compares the flight tracking performance with and without the use of the GLA term. In Figure 3 the flight path angle, which is to be maintained at zero, is compared. The deviations from zero are seen to be slightly less extreme in the GLA on case. Figure 4 compares the elevator deflection governed by the nominal tracking controller in each of the two cases. Note that the commanded deflection is larger when GLA is active which is expected since the nominal controller will try to offset the VCCTEF action of the GLA controller. Figure 5 again shows the reduction in the performance metric M_y when

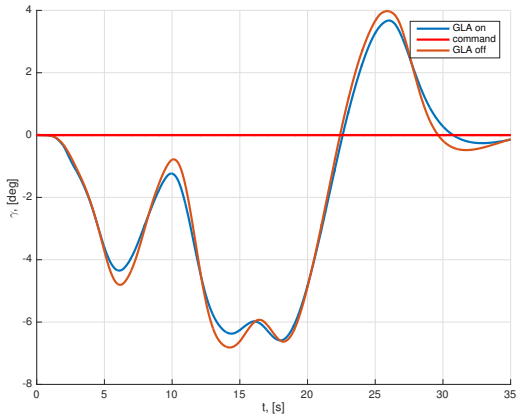

Figure 3. Flight path angle comparison with GLA controller on and GLA controller off

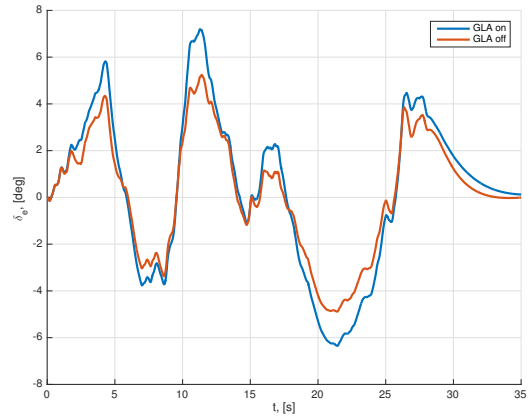

Figure 4. Elevator deflection comparison with GLA controller on and GLA controller off

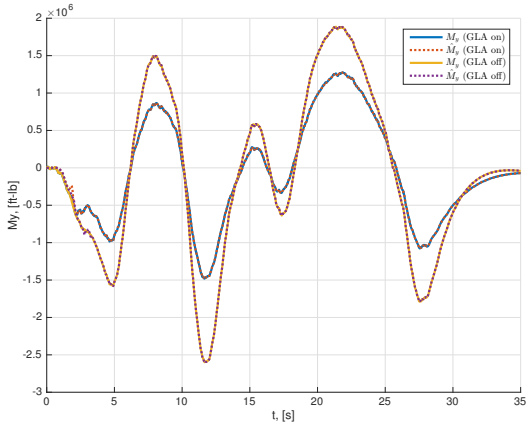

Figure 5. Wing root bending moment comparison with GLA controller on and GLA controller off

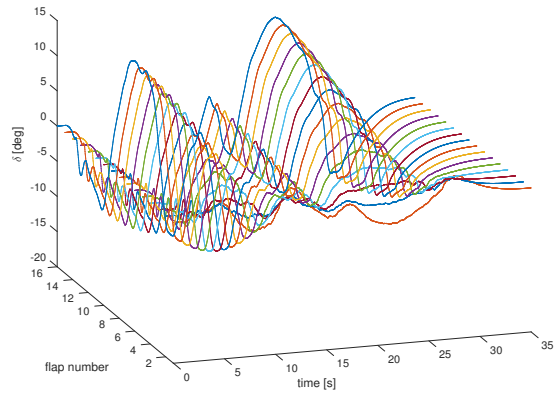

Figure 6. Commanded VCCTEF deflections with GLA controller on

the GLA control term is used. The image also shows how the $\hat{M}_y$ estimate compares to the actual M_y measurement. Good agreement is seen after a brief transient in both cases, but note that this does not imply that the wing root bending moment system matrix estimates match their true values element-wise. Finally, Figure 6 shows the deflection of each VCCTEF segment with the GLA controller on. The 16 control signals are recovered from the 4 virtual control variables and the Chebyshev polynomial shape function described in Section IV.A. They form a relatively smooth surface that facilitates satisfaction of the relative deflection limits between segments.

Finally, consider the same simulation using the extended state observer described in Section III.D to estimate $\hat{w}$ instead of of the adaptive approach in Section III.C. The same measurements are used to drive the observer and all tuning parameters and initial conditions are set to the same values for the $q = 1e - 9$ case. The mapping of Eq. (40) is used in the extended state observer implementation. Figure 7 shows the evolution of the norm of the error between w and $\hat{w}$ when using the adaptive estimation scheme and when using the extended state observer. No significant advantage appears to be offered by either method in this case. The corresponding time history of M_y for each of the two estimation methods is shown in 8. Little difference is seen in the performance metric, as expected from the similarly inaccurate $\hat{w}$ estimates. Without additional measurements, especially those from gust-dedicated sensors, or a more sophisticated disturbance reconstruction scheme the choice of estimation method is not a notable design consideration for the stated problem structure.

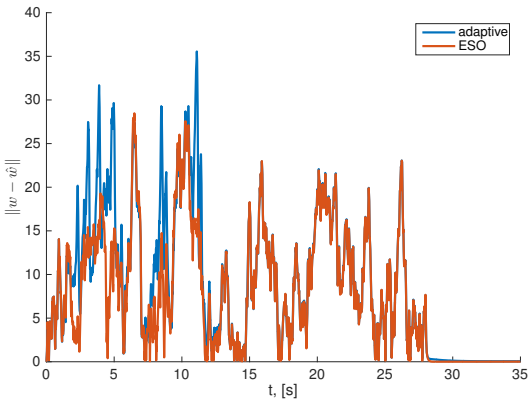

Figure 7. Disturbance estimate error with adaptive estimation vs. extended state observer

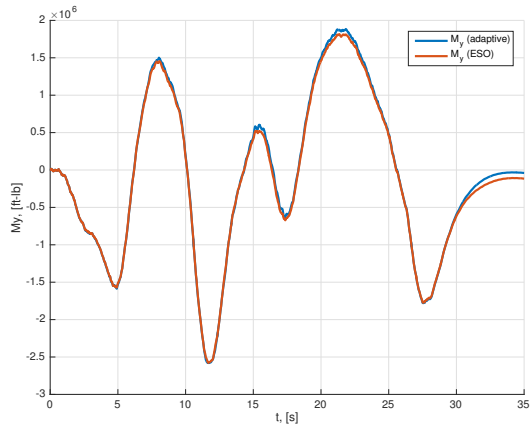

Figure 8. Wing root bending moment using disturbance estimate from adaptive estimation vs. extended state observer

V. Conclusion

This paper presents a gust load alleviating control design for use with next generation flexible wing aircraft. The design makes use of a continuous trailing edge control surface that can provide wing shaping functionality. An appropriate control signal is obtained from the optimal control solution to a multi-objective cost function that involves unknown parameters. The unknown quantities must be updated online, requiring a Riccati equation to be solved at each time step and resulting in time-varying control gains. The control design was simulated on a flexible wing aircraft model in gust-disturbed level flight and seen to notably reduce the load experienced by the wing when compared to use of a traditional control design alone. Performance using two disturbance estimation schemes was compared, but both methods offered similar performance

In the future, variations to the multi-objective statement will be explored. The performance improvement obtained using other methods of estimating the disturbance signal or utilizing performance metrics besides wing root bending moment could be compared. The design could also be made adaptive in an attempt to compensate for disturbance estimation error with the time-varying closed-loop system serving as a reference model.

Acknowledgments

This work was supported by an appointment to the NASA Postdoctoral Program at the NASA Ames Research Center, administered by Universities Space Research Association under contract with NASA. Additional funding was provided by the Advanced Air Transport Technology Project of the NASA Aeronautics Research Mission Directorate.

References

[1]Nguyen, N., and Urnes, J., "Aeroelastic modeling of elastically shaped aircraft concept via wing shaping control for drag reduction," AIAA Atmospheric Flight Mechanics Conference, AIAA 2012-4642, August 2012.

[2]Nguyen, N., and Tal, E., "A multi-objective flight control approach for performance adaptive aeroelastic wing,"56th AIAA/ASCE/AHS/ASC Structures, Structural Dynamics, and Materials Conference, AIAA 2015-1843, January 2015.

[3]Nguyen, N., Ting, E., Chaparro, D., Drew, M., and Swei, S., "Multi-objective flight control from drag minimization and load alleviation of high-aspect ration flexible wing aircraft," 58th AIAA/ASCE/AHS/ASC Structures, Structural Dynamics, and Materials Conference, AIAA 2017-1589, January 2017.

[4]Nguyen, N., Hashemi, K., Yucelen, T., and Arabi, E., "Performance optimizing multi-objective adaptive control with time-varying model reference modification," AIAA Guidance, Navigation, and Control Conference, AIAA 2017-1715, January 2017.

[5]Nguyen, N., "Elastically shaped future air vehicle concept," NASA Innovation Fund Award 2010 Report, October 2010, Submitted to NASA Innovative Partnerships Program, http://ntrs.nasa.gov/archive/nasa/casi.ntrs.nasa.gov/20110023698.pdf.

[6]Nguyen, N., Trinh, K., Reynolds, K., Kless, J., Aftosmis, M., Urnes, J., Ippolito, C., "Elastically shaped wing optimization and aircraft concept for improved cruise efficiency," AIAA Aerospace Sciences Meeting, AIAA 2013-0141, January 2013.

[7]Boeing Report No. 2012X0015, "Development of variable camber continuous trailing edge flap system," October 4, 2012.

[8]Urnes, J., Nguyen, N., Ippolito, C., Totah, J., Trinh, K,. and Ting, E., "A mission adaptive variable camber flap control system to optimize high lift and cruise lift to drag ratios of future N+3 transport aircraft," AIAA Aerospace Sciences Meeting, AIAA 2013-0214, January 2013.

[9]Hoblit, F.M., *Gust loads on Aircraft: Concepts & applications*, AIAA, Washington, DC, 1988.

[10]Ting, E., Chaparro, D., Nguyen, N., "Development of an integrated nonlinear aeroservoelastic flight dynamic model of the truss-braced wing aircraft," 58th AIAA/ASCE/AHS/ASC Structures, Structural Dynamics, and Materials Conference, AIAA 2017-1815, January 2017.